Single-knob beam line for transverse emittance partitioning

C. Xiao and O. K. Kester
Institut für Angewandte Physik, Goethe Universität, D-60483 Frankfurt am Main, Germany

L. Groening, H. Leibrock, M. Maier, and P. Rottländer
GSI Helmholtzzentrum für Schwerionenforschung GmbH, D-64291 Darmstadt, Germany
(Received 10 December 2012; revised manuscript received 25 March 2013; published 11 April 2013)

Flat beams feature unequal emittances in the horizontal and vertical phase space. Such beams were created successfully in electron machines by applying effective stand-alone solenoid fringe fields in the electron gun. Extension of this method to ion beams was proposed conceptually. The present paper is on the decoupling capabilities of an ion beam emittance transfer line. The proposed beam line provides a single-knob tool to partition the horizontal and vertical rms emittances, while keeping the product of the two emittances constant as well as the transverse rms Twiss parameters ($\alpha_{x,y}$ and $\beta_{x,y}$) in both planes. It is shown that this single knob is the solenoid field strength.

DOI: 10.1103/PhysRevSTAB.16.044201 PACS numbers: 41.75.Ak, 41.85.Ct, 41.85.Ja

I. INTRODUCTION

The modification of projected beam emittances under preservation of the full six-dimensional emittance became a matter of interest for many accelerator applications. First experiments were proposed and conducted in [1,2] at electron machines about a decade ago. The issue is of special interest for increasing the performance of x-ray free electron lasers and advanced approaches to emittance repartitioning are under conceptual and experimental investigation [3–8]. Flat hadron beams could facilitate the process of multiturn injection into circular machines, which imposes different requirements on the horizontal and vertical emittance of the incoming beam. Recently, it was proposed to use flat beams in hadron-hadron collisions to provide higher luminosity by mitigating beam-beam effects [9,10]. The mass resolution of spectrometers is increased significantly if the beam is flat perpendicular to the direction of the spectrometers bend. A corresponding setup behind an electron-cyclotron-resonance source is proposed in [11].

From first principles beams are created round without any coupling among planes. Their rms emittances as well as their eigen-emittances are equal in the two transverse planes. Thus, any transverse round-to-flat transformation requires a change of the beam eigen-emittances by a nonsymplectic transformation [12]. Such a transformation can be performed by placing a charge state stripper inside an axial magnetic field region as proposed in [13]. Inside such a solenoid stripper, transverse interplane correlations are created nonsymplectically. Afterwards they are removed symplectically by a decoupling section including skew quadrupoles. It must be mentioned that the use of charge state strippers (outside from solenoids) is state of the art at several ion machines that provide highly charged ions [14–16].

It is emphasized that the paper is on the application of coupled beam dynamics aiming for increased performance of an accelerator chain. It is not on coupled beam dynamics theory itself and references are given whenever needed. The paper starts with a reintroduction of the required terms of coupled beam dynamics. Afterwards the beam line for transverse emittance transfer is presented. The fourth section is on modeling the nonsymplectic process of charge state stripping inside a solenoid followed by the treatment of the symplectic decoupling section. The decoupling and matching capabilities of the setup are remarkably flexible and the impact and discussion of these findings are treated in dedicated sections. The paper puts some emphasis on the detailed description of the beam line and beam parameters since its decoupling and matching features were found within the preparation of the experimental proof of principle of emittance transfer by means of tracking simulations.

II. BASIC TERMS

The four-dimensional symmetric beam matrix

$$C = \begin{bmatrix} \langle xx \rangle & \langle xx' \rangle & \langle xy \rangle & \langle xy' \rangle \\ \langle x'x \rangle & \langle x'x' \rangle & \langle x'y \rangle & \langle x'y' \rangle \\ \langle yx \rangle & \langle yx' \rangle & \langle yy \rangle & \langle yy' \rangle \\ \langle y'x \rangle & \langle y'x' \rangle & \langle y'y \rangle & \langle y'y' \rangle \end{bmatrix} \quad (1)$$

contains ten unique elements, four of which describe the coupling. If at least one of the elements of the off-diagonal submatrix is nonzero, the beam is x-y coupled. The four-dimensional rms emittance ε_{4d} is the square root of the determinant of C, and the projected beam rms emittances

ε_x and ε_y are the square roots of the determinants of the on-diagonal submatrices, i.e., phase space area divided by π. Diagonalization of the beam matrix yields the eigen-emittances ε_1 and ε_2,

$$\bar{C} = MCM^T = \begin{bmatrix} \varepsilon_1 & 0 & 0 & 0 \\ 0 & \varepsilon_1 & 0 & 0 \\ 0 & 0 & \varepsilon_2 & 0 \\ 0 & 0 & 0 & \varepsilon_2 \end{bmatrix}, \tag{2}$$

with

$$\varepsilon_1 = \tfrac{1}{2}\sqrt{-\mathrm{tr}[(CJ)^2] + \sqrt{\mathrm{tr}^2[(CJ)^2] - 16\det(C)}}, \tag{3}$$

$$\varepsilon_2 = \tfrac{1}{2}\sqrt{-\mathrm{tr}[(CJ)^2] - \sqrt{\mathrm{tr}^2[(CJ)^2] - 16\det(C)}}, \tag{4}$$

as shown in Appendix A. The four-dimensional matrix J is the skew-symmetric matrix with nonzero entries on the block diagonal off form. Any symplectic transformation M obeys

$$M^T J M = J, \qquad J = \begin{bmatrix} 0 & 1 & 0 & 0 \\ -1 & 0 & 0 & 0 \\ 0 & 0 & 0 & 1 \\ 0 & 0 & -1 & 0 \end{bmatrix}. \tag{5}$$

Eigen-emittances are invariant under symplectic transformations and the eigen-emittances are equal to the rms emittances if and only if interplane correlations are zero.

III. EMITTANCE TRANSFER BEAM LINE

The planned emittance transfer experiment (EMTEX) beam line for the demonstration of transverse rms emittance transfer is shown in Fig. 1. The EMTEX section comprises two quadrupole doublets, a solenoid with stripper foil inside, a quadrupole triplet, a skew quadrupole triplet, another quadrupole triplet, a current transformer, and a transverse emittance measurement unit. Its total length is about 13 m. Centering of the beam can be done through a grid a few meters in front of the first doublet, the grid of the emittance measurement setup, and finally by observing the foil on-line, i.e., the light emission from the impacting beam.

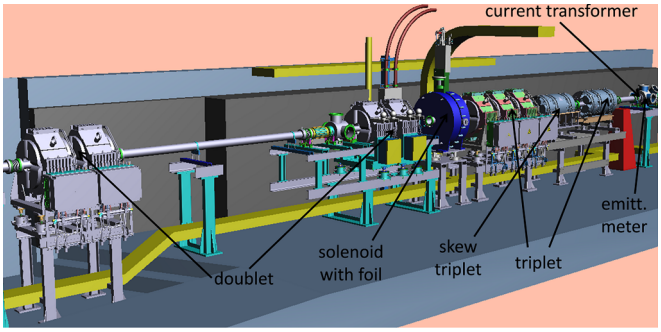

FIG. 1. Layout of the EMTEX section.

In order to mitigate four-dimensional rms emittance growth from scattering during the stripping process, the beam sizes on the stripper foil should be kept as small as possible. Two quadrupole doublets separated by a drift space in front of the solenoid do the required matching. A low intensity beam of D_6^+ [17,18], previously accelerated to 11.4 MeV/u at 108 MHz and stripped to $3D_2^+$ in a 22 μg/cm^2 carbon foil placed at the center of a solenoid will be used, and the total relative momentum spread of the beam is less than $\pm 5 \times 10^{-4}$ as verified by Schottky spectra in the synchrotron served by our linac. The maximum longitudinal magnetic field is 1.0 T. This nonsymplectic transformation creates x-y coupling between the transverse planes. The nonsymplecticity is from omission of parts of the full system comprising the stripping process. It includes the incoming beam particle nuclei, their residual electrons, and the nuclei and electrons of the stripping foil atoms. However, for the beam dynamics just the stripped beam ions are kept in the system. The stripping atoms and the stripped-off electrons are removed artificially from the system. This removal is nonsymplectic.

A quadrupole triplet and a skew quadrupole triplet separated by a drift space are employed to remove these correlations symplectically. The section from the solenoid exit to the skew triplet exit will be called decoupling section in the following. A final quadrupole triplet is used for matching to the existing beam line followed by a beam current transformer and an emittance measurement unit. The full beam line is presented quantitatively in Appendix B.

IV. STRIPPING INSIDE A SOLENOID

Stripping inside a solenoid is fundamentally different from stripping between two solenoids due to the longitudinal magnetic field component and the fringe fields. In case of pure transverse field components (dipoles, quadrupoles, n-poles), there is equivalence between stripping inside this magnet and stripping between two such magnets of half lengths.

Let C_0 denote the second moment matrix at the entrance of the solenoid. If the beam has equal horizontal and vertical rms emittances and no interplane correlations, the beam matrix can be simplified to (in the case here, $\alpha_{x,y} = 0$)

$$C_0 = \begin{bmatrix} \varepsilon\beta & 0 & 0 & 0 \\ 0 & \frac{\varepsilon}{\beta} & 0 & 0 \\ 0 & 0 & \varepsilon\beta & 0 \\ 0 & 0 & 0 & \frac{\varepsilon}{\beta} \end{bmatrix}. \tag{6}$$

Assuming a very short solenoid, its transfer matrix can be divided into two parts:

$$R_{\text{in}} = \begin{bmatrix} 1 & 0 & 0 & 0 \\ 0 & 1 & k_{\text{in}} & 0 \\ 0 & 0 & 1 & 0 \\ -k_{\text{in}} & 0 & 0 & 1 \end{bmatrix}, \qquad R_{\text{out}} = \begin{bmatrix} 1 & 0 & 0 & 0 \\ 0 & 1 & -k_{\text{out}} & 0 \\ 0 & 0 & 1 & 0 \\ k_{\text{out}} & 0 & 0 & 1 \end{bmatrix}. \tag{7}$$

If the beam rigidity does not change inside the solenoid, k_{in} is equal to k_{out}, and $k_{\text{in}} = k_{\text{out}} = k$. The first part describes the entrance fringe field and the second part is the exit fringe field. In here the focusing strength of the solenoid is

$$k = \frac{B}{2(B\rho)}. \tag{8}$$

B is the on-axis magnetic field strength and $B\rho$ is the beam rigidity. The beam matrix C_1 after the entrance fringe field k is found as

$$C_1 = R_{\text{in}} C_1 R_{\text{in}}^T = \begin{bmatrix} \varepsilon\beta & 0 & 0 & -k\varepsilon\beta \\ 0 & \frac{\varepsilon}{\beta} + k^2\varepsilon\beta & k\varepsilon\beta & 0 \\ 0 & k\varepsilon\beta & \varepsilon\beta & 0 \\ -k\varepsilon\beta & 0 & 0 & \frac{\varepsilon}{\beta} + k^2\varepsilon\beta \end{bmatrix}. \tag{9}$$

The off-diagonal submatrices describe the correlations and the values of $\langle xy \rangle$ and $\langle x'y' \rangle$ are zero. In order to change the eigen-emittances, a nonsymplectic transformation has to be integrated into the round-to-flat transformation section. The nonsymplectic transformation is accomplished for instance by changing the beam rigidity $B\rho$ in between the fringe fields from $(B\rho)_{\text{in}}$ to $(B\rho)_{\text{out}}$ through charge state stripping. Defining

$$\delta q := \frac{(B\rho)_{\text{in}}}{(B\rho)_{\text{out}}}, \tag{10}$$

the exit fringe field transfer matrix changes to ($k_{\text{in}} = k$, $k_{\text{out}} = \delta q k$)

$$R'_{\text{out}} = \begin{bmatrix} 1 & 0 & 0 & 0 \\ 0 & 1 & -\delta q k & 0 \\ 0 & 0 & 1 & 0 \\ \delta q k & 0 & 0 & 1 \end{bmatrix}. \tag{11}$$

The focusing strength k of the solenoid is calculated from the unstripped charge state. The elements of the beam matrix C'_1 directly after the stripper foil inside of the solenoid but still before the exit fringe field are

$$C'_1 = \begin{bmatrix} \varepsilon\beta & 0 & 0 & -k\varepsilon\beta \\ 0 & \frac{\varepsilon}{\beta} + k^2\varepsilon\beta + \Delta\varphi^2 & k\varepsilon\beta & 0 \\ 0 & k\varepsilon\beta & \varepsilon\beta & 0 \\ -k\varepsilon\beta & 0 & 0 & \frac{\varepsilon}{\beta} + k^2\varepsilon\beta + \Delta\varphi^2 \end{bmatrix} \tag{12}$$

with stripping scattering effects on the angular spread being included. The parameter $\Delta\varphi^2$ is the scattering amount during the stripping process [19], and the stripper foil itself is modeled by increasing the spread of the angular distribution through scattering. After the stripper foil the beam passes through the exit fringe field with reduced beam rigidity and the beam matrix C'_2 after the exit fringe field becomes

$$C'_2 = R'_{\text{out}} C'_1 R'^T_{\text{out}} = \begin{bmatrix} \varepsilon_n R_n & ak\varepsilon_n\beta_n J_n \\ -ak\varepsilon_n\beta_n J_n & \varepsilon_n R_n \end{bmatrix}, \tag{13}$$

where $a := \delta q - 1$ and

$$\varepsilon_n = \sqrt{\varepsilon\beta\left(\frac{\varepsilon}{\beta} + a^2k^2\varepsilon\beta + \Delta\varphi^2\right)}, \qquad \beta_n = \frac{\beta\varepsilon}{\varepsilon_n}, \tag{14}$$

introducing the 2×2 submatrices R_n and J_n:

$$R_n = \begin{bmatrix} \beta_n & 0 \\ 0 & \frac{1}{\beta_n} \end{bmatrix}, \qquad J_n = \begin{bmatrix} 0 & 1 \\ -1 & 0 \end{bmatrix}. \tag{15}$$

The amount of eigen-emittance transfer scales with the longitudinal magnetic field strength and the beam rms sizes on the stripper. Interplane correlations are created and the rms emittances and eigen-emittances after the solenoid with stripper foil read

$$\varepsilon_{x,y} = \varepsilon_n, \qquad \varepsilon_{1,2} = \varepsilon_n(1 \pm ak\beta_n). \tag{16}$$

The parameter t is introduced to quantify the interplane coupling. If t defined as

$$t = \frac{\varepsilon_x\varepsilon_y}{\varepsilon_1\varepsilon_2} - 1 \geq 0 \tag{17}$$

is equal to zero, there are no interplane correlations and the beam is fully decoupled. Kim [20] introduced the beam angular momentum $2\xi = \langle xy' - x'y \rangle$ and for an angular momentum dominated beam one finds $t = \xi^2/\varepsilon_{4d}$. After the solenoid exit fringe field, the t value can be calculated as

$$t = \frac{a^2 k^2 \varepsilon \beta}{\frac{\varepsilon}{\beta} + \Delta\varphi^2} \tag{18}$$

and the four-dimensional rms emittance is

$$\varepsilon_{4d} = \varepsilon_1 \varepsilon_2 = \varepsilon^2 + \varepsilon\beta\Delta\varphi^2. \tag{19}$$

Obtaining this result we neglected the finite solenoid length, i.e., its central pure longitudinal magnetic field. Tracking simulations using three-dimensional magnetic field maps of finite solenoids confirmed that this omission is justified [21,22]. The four-dimensional rms emittance increase is proportional to the beam sizes on the stripper foil. It is purely from scattering in the foil; it is not caused by the shift of beam rigidity inside the longitudinal magnetic field.

V. DECOUPLING SECTION

The simplest skew decoupling section only contains three skew quadrupoles with appropriate betatron phase advances in each plane [23,24]. Let R_q be the 4×4 matrix corresponding to a certain arrangement of quadrupoles and drift spaces and assume that this channel is represented by an identity matrix in the x direction and has an additional 90° phase advance in the y direction as in [20]

$$R_q = \begin{bmatrix} I_n & O_n \\ O_n & T_n \end{bmatrix}. \tag{20}$$

Here the 2×2 submatrices O_n, T_n, and I_n are defined as

$$O_n = \begin{bmatrix} 0 & 0 \\ 0 & 0 \end{bmatrix}, \quad T_n = \begin{bmatrix} 0 & u \\ -\frac{1}{u} & 0 \end{bmatrix}, \quad I_n = \begin{bmatrix} 1 & 0 \\ 0 & 1 \end{bmatrix}. \tag{21}$$

If the quadrupoles are tilted by 45°, the 4×4 transfer matrix can be written as

$$\bar{R} = R_r R_q R_r^T = \frac{1}{2}\begin{bmatrix} T_{n+} & T_{n-} \\ T_{n-} & T_{n+} \end{bmatrix}, \tag{22}$$

where

$$R_r = \frac{\sqrt{2}}{2}\begin{bmatrix} I_n & I_n \\ -I_n & I_n \end{bmatrix}, \qquad T_{n\pm} = T_n \pm I_n. \tag{23}$$

The beam matrix C_3' after the decoupling section is

$$C_3' = \bar{R} C_2' \bar{R}^T = \begin{bmatrix} \eta_+ \Gamma_{n+} & \zeta \Gamma_{n-} \\ \zeta \Gamma_{n-} & \eta_- \Gamma_{n+} \end{bmatrix}, \tag{24}$$

and the 2×2 submatrices $\Gamma_{n\pm}$ are defined through

$$\Gamma_{n\pm} = \begin{bmatrix} u & 0 \\ 0 & \pm\frac{1}{u} \end{bmatrix}, \tag{25}$$

with

$$\eta_\pm = \frac{\varepsilon_n}{2}\left(\frac{\beta_n}{u} + \frac{u}{\beta_n} \pm 2ak\beta_n\right), \tag{26}$$

and

$$\zeta = \frac{\varepsilon_n}{2}\left(-\frac{\beta_n}{u} + \frac{u}{\beta_n}\right). \tag{27}$$

Assuming that this beam matrix is diagonal, its x-y component vanishes:

$$\zeta \Gamma_{n-} = O_n \tag{28}$$

solved by

$$u = \beta_n. \tag{29}$$

This result was found earlier in [20] for instance. However, the major steps have been repeated here since they will be referred to later. Suppose that the decoupling transfer matrix $\bar{R}$ is able to decouple the two transverse planes of C_2'. We still do not know how this transfer beam line looks in detail, but anyway we calculate the final rms emittances obtaining

$$\varepsilon_{x,y} = \frac{\varepsilon_n}{2}\left(\frac{\beta_n}{u} + \frac{u}{\beta_n} \pm 2ak\beta_n\right). \tag{30}$$

This idealized example serves illustrating the principle, and it may be accomplished with just three skew quadrupoles. For a given solenoid strength k_0, referring to the unstripped beam, the corresponding quadrupole gradients of the decoupling section are determined using a numerical routine, such that finally the rms emittances are equal to the eigenemittances. If these optimized gradients are applied to remove interplane correlations produced by a different solenoid strength k_1, the resulting rms emittances and eigenemittances at the exit of the decoupling section are calculated to be

$$\varepsilon_{x,y} = \frac{\varepsilon_n(k_1)}{2}\left[\frac{\beta_n(k_1)}{\beta_n(k_0)} + \frac{\beta_n(k_0)}{\beta_n(k_1)} \pm 2ak_1\beta_n(k_1)\right] \tag{31}$$

and

$$\varepsilon_{1,2} = \varepsilon_n(k_1)[1 \pm ak_1\beta_n(k_1)] \tag{32}$$

with the parameter t:

$$t = \frac{a^4\varepsilon^2\beta^2}{(\frac{\varepsilon}{\beta} + \Delta\varphi^2)(\frac{\varepsilon}{\beta} + a^2k_0^2\varepsilon\beta + \Delta\varphi^2)} \frac{(k_1^2 - k_0^2)^2}{4}. \tag{33}$$

In the same way the rms Twiss parameters of a beam coupled by k_1 but decoupled by $\bar{R}(k_0)$ are found from Eq. (24) as

$$\tilde{\alpha}_x = \tilde{\alpha}_y = 0, \qquad \tilde{\beta}_x = \tilde{\beta}_y = \beta_n(k_0), \tag{34}$$

showing that the rms Twiss parameters after decoupling section do not depend on the coupling solenoid strength k_1

if the decoupling section was set assuming a coupling strength k_0.

The EMTEX beam line uses more elements than a single skew triplet because of finite apertures and gradients of a real experiment. Its decoupling section comprises a quadrupole triplet and a skew quadrupole triplet separated by a drift. The quadrupole gradients are optimized numerically from a numerical routine [13] to remove the interplane correlations thus minimizing the horizontal (for instance) rms emittances to the lower of the eigen-emittances.

Figure 2 illustrates the transverse emittance transfer and the multiparticle beam dynamics simulations have been done using the TRACK code [25]. The relevant parameters of the simulations are summarized in Appendix B. In the first step we assume that the and the skew quadrupole triplet are turned off. This process is an ordinary stripping process and the eigen-emittances are equal to the rms emittances at the entrance and exit of this section. It reflects today's situation of providing highly charged ions from linacs. Because of the stripping growth of eigen-emittances and rms emittances is unavoidable. It is the reference scenario to which the transverse rms emittance transfer scenario is to be compared.

In the latter case, the solenoid and the skew quadrupoles triplet are turned on. Once the beam enters the entrance fringe field of the solenoid, the eigen-emittances start to split gradually. After stripping, the exit fringe field of the solenoid is passed by the beam with reduced beam rigidity, thus overcompensating the previous eigen-emittance separation; the eigen-emittances diverge inside the solenoid and are preserved afterwards. Along the decoupling skew quadrupole triplet the rms emittances are made equal to the separated eigen-emittances. Compared to the reference scenario, the final horizontal rms emittance is reduced significantly.

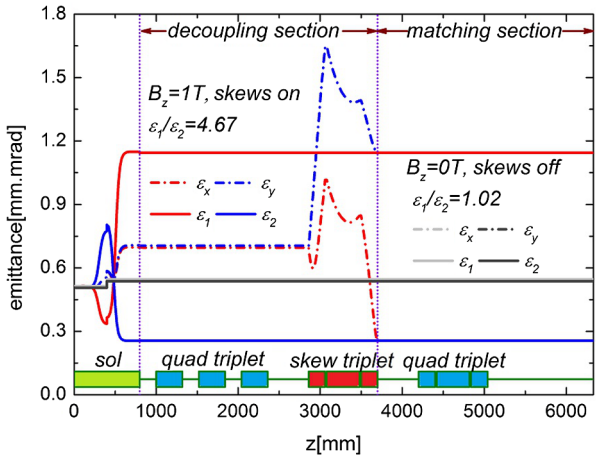

FIG. 2. Evolution of the rms emittances and eigen-emittances along the EMTEX beam lines for two cases: in the first case (reference, gray and black lines) the solenoid and the skew quadrupoles are off, i.e., no nonsymplectic action nor coupling. Eigen-emittances and rms emittances are always equal and they change just during the stripping from angular scattering. In the second case (red and blue lines) the solenoid field is 1.0 T and its fringes cause nonsymplectic actions that change the eigen-emittances. Eigen-emittances and rms emittances separate and both are increased during stripping. The skew quadrupoles are turned on as well and remove the coupling previously produced inside of the solenoid. Since skew quadrupoles are symplectic, they do not change the eigen-emittances. After this decoupling the rms emittances are equal to the nonsymplectically changed eigen-emittances.

Therefore, this emittance transfer experiment is therefore fundamentally different from an emittance exchange experiment. Emittance transfer is nonsymplectic and the amount of transfer can be controlled by the solenoid field strength and the beam size on the stripping foil. Behind the decoupling section another regular quadrupole triplet is required to rematch the beam for further transport.

VI. DECOUPLING CAPABILITY ANALYSIS

EMTEX will use a beam of molecules from D_6^+ with the initial beam parameters $\alpha = 0$, $\beta = 2.5$ mm/mrad, and $\varepsilon = 0.51$ mm mrad at the entrance of the solenoid. The stripping scattering amount $\Delta\varphi$ is 0.226 mrad [19] and the decoupling transfer matrix is determined for 1.0 T of solenoid field. The eigen-emittances and rms emittances at the exit of the solenoid calculated using Eq. (16) and those obtained from tracking through three-dimensional field maps are compared in Fig. 3. The beam is strongly coupled.

For the simplest decoupling transfer matrix, the decoupling section is composed of a skew quadrupole triplet, explicitly from Eq. (22) (in units of mm and mrad):

$$\bar{R}_{\text{simplest}} = \begin{bmatrix} +0.500 & +0.891 & -0.500 & +0.891 \\ -0.281 & +0.500 & -0.281 & -0.500 \\ -0.500 & +0.891 & +0.500 & +0.891 \\ -0.281 & -0.500 & -0.281 & +0.500 \end{bmatrix}. \quad (35)$$

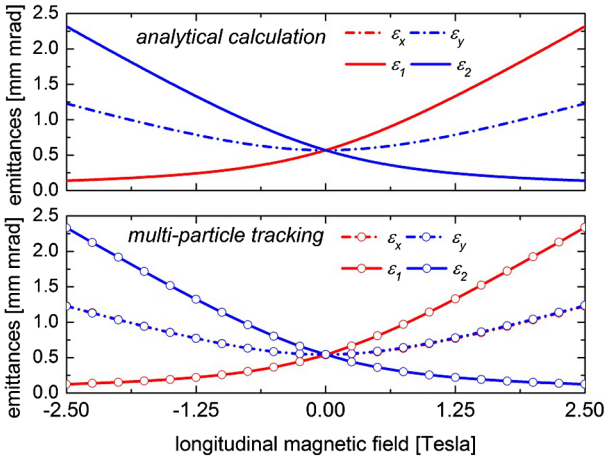

FIG. 3. Eigen-emittances and rms emittances calculated by the analytical method based on the short solenoid transfer matrix of Eq. (16) and by multiparticle tracking through three-dimensional field maps.

The EMTEX decoupling section comprises a quadrupole triplet and a skew quadrupole triplet separated by a drift. Therefore, its decoupling transfer matrix has a more complex structure, explicitly (in units of mm and mrad)

$$\bar{R}_{\mathrm{EMTEX}} = \begin{bmatrix} +0.386 & -0.548 & -0.240 & -0.647 \\ +1.304 & -0.535 & -0.111 & -2.348 \\ +0.673 & +0.126 & -0.161 & +1.301 \\ +0.389 & +0.805 & -0.495 & +0.846 \end{bmatrix}, \quad (36)$$

being different from the form of Eq. (22). The final eigen-emittances and rms emittances at the exit of the skew quadrupole triplet calculated using Eq. (22) and those obtained from tracking through the EMTEX beam line are compared in Fig. 4. For the simple decoupling section the calculation is based on the transfer matrix method of Eq. (22). For the EMTEX decoupling section multiparticle tracking through the external three-dimensional field maps (for the solenoid) and the external one-dimensional field profile (for the quadrupole and skew quadrupole) were adopted.

The remarkable result is that both decoupling matrices work effectively for a wide range of longitudinal magnetic field values, i.e., the beam is well decoupled for a wide range of longitudinal magnetic fields around the field the quadrupoles have been optimized for. Additionally, in both cases the decoupling performance is independent from the sign of k_1 as suggested by Eq. (33) and weakly depended on $(k_1\text{-}k_0)$. We currently do not have a complete analytical understanding of this weak dependence except for the simple decoupling matrix Eq. (22). However, we still aim for understanding why the dependence is so weak even for the EMTEX decoupling beam line being more complex with respect to (wrt) Eq. (22). To exclude that this is casual for this one beam line, the beam line has been modified by prolonging or shortening drifts and quadrupole field lengths. For all modifications (all using a regular quadrupole triplet followed by a skew quadrupole triplet), the same behavior of decoupling performance was observed.

However, this behavior simplifies the decoupling significantly as readoption of gradients to the solenoid field can be skipped within a reasonable range of solenoid fields. It provides a single-knob tool to partition the horizontal and vertical beam rms emittances. The behavior of t calculated analytically by Eq. (22) and by tracking through EMTEX is illustrated in Fig. 5, where the stripping scattering amount $\Delta\varphi$ is 0.226 mrad and the longitudinal magnetic field is varied. At EMTEX k_0 corresponds to a solenoid field of 1.0 T and accordingly t has a minimum for that value. The beam is well decoupled for a wide range of solenoid fields for both the analytical calculation and for tracking through the EMTEX beam line.

The dependence of t on the solenoid field as obtained from tracking has been fitted with a 4th order polynomial as motivated by Eq. (33) and the fit is plotted as well in Fig. 5. This result might suggest a general 4th order dependence of the decoupling performance of any beam line on the coupling-driving solenoid field. The analytical investigation of this suggestion is ongoing. During the experimental proof of eigen-emittance tayloring with effective fringe fields by Piot *et al.* [5], the authors used the beam size to control the amount of eigen-emittance change. EMTEX will use the solenoid field strength instead. Using the beam size, the decoupling gradients must be readopted to the specific beam size.

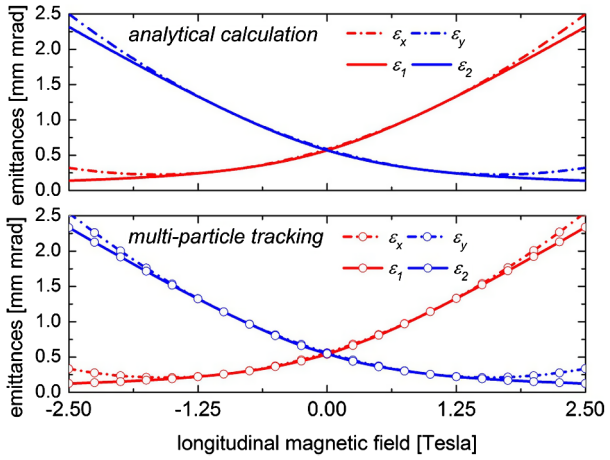

FIG. 4. Eigen-emittances and rms emittances calculated by the analytical method based on the decoupling matrix of Eq. (22) and by multiparticle tracking through the EMTEX beam line. Although the longitudinal magnetic field is varied, the decoupling gradients are kept constant at the values determined to decouple the beam coupled by a longitudinal magnetic field of 1.0 T.

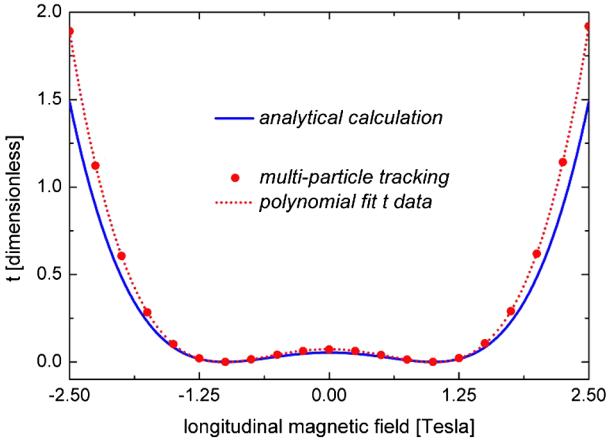

FIG. 5. The parameter t calculated analytically and by multiparticle tracking simulation. Although the longitudinal magnetic field is varied, the decoupling gradients are kept constant at the values determined to decouple the beam coupled by a longitudinal magnetic field of 1.0 T.

Within the preparation of experimental investigation of the decoupling at EMTEX, machine-related error studies wrt quadrupole gradients and rolls were done. As shown in [22], just rolls have a notable but negligible effect on the decoupling.

VII. MATCHING CAPABILITY ANALYSIS

Another convenient feature of EMTEX, which can be explained for the generic case of decoupling according to Eq. (22), seems to manifest as a general rule in numerical matrix as well as in tracking calculations. Its generality we cannot explain for the time being: the shape of the transverse beta functions after the decoupling section does not practically depend on the solenoid field strength. In other words, the two transverse rms ellipses after decoupling are just changed in size through the solenoid field; their orientation and shape remains unaffected by the solenoid strength. This matching capability of EMTEX is illustrated in Figs. 6 and 7.

This feature has some analogy to an achromatic section. Inside an achromat the dispersion functions D and D' are nonzero and the envelope shapes depend on the amount of momentum spread. Behind an achromat D and D' are zero and envelopes do not depend (to first order) any longer on the momentum spread. As mentioned before, we do not fully understand yet this analogy and its complete investigation shall be beyond the scope of this paper.

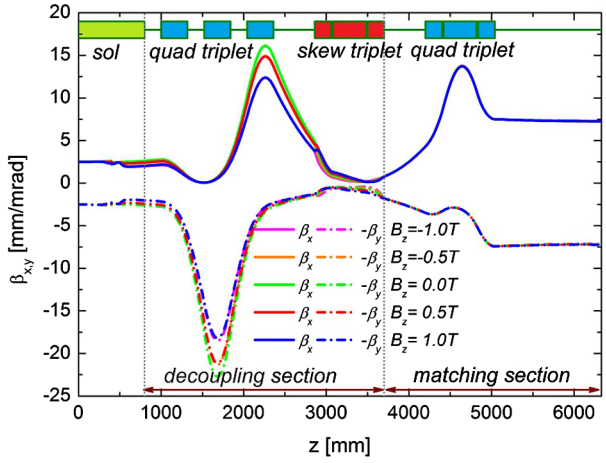

FIG. 6. Horizontal and vertical beta functions of the beam along the EMTEX beam line for different solenoid field strengths. The gradients of all quadrupoles (regular and skew) are constant. The shape of the horizontal and vertical beta function does depend on the solenoid field strength just between the solenoid entrance and the exit of the last skew quadrupole, i.e., along the part of the beam line where interplane coupling is nonzero. Behind the last skew quadrupole all coupling is removed and from this position on the shape of the beta function is invariant under solenoid field strength variation.

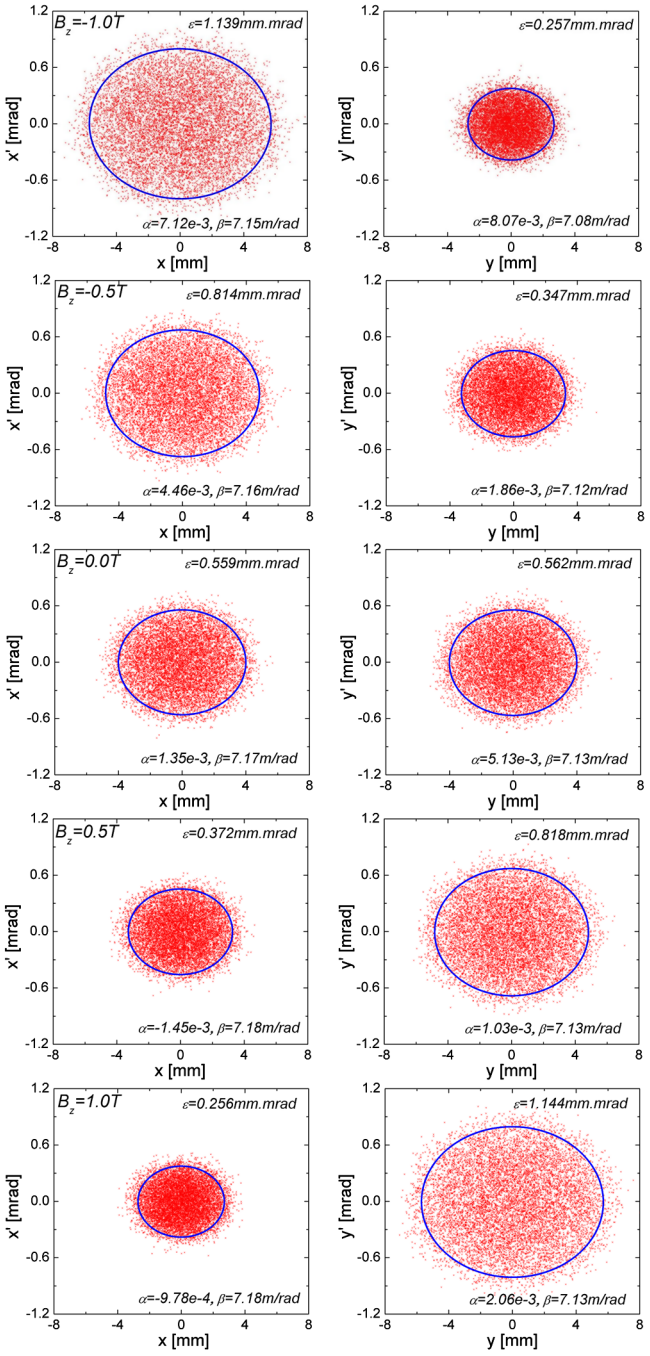

FIG. 7. The transverse emittance portraits at the exit of the beam line for different solenoid field strengths. The gradients of the quadrupoles and skew quadrupoles are constant. The rms Twiss parameters do not depend on the solenoid field strength.

VIII. CONCLUSION AND OUTLOOK

A beam line for demonstration of round-to-flat transformation of an initially uncoupled ion beam was presented. It comprises two doublets for matching the required beam parameters on a stripping foil being placed in the center of a solenoid. The net effect on the beam is a nonsymplectic transformation creating interplane cou-

pling, being removed afterwards along a beam line from one regular quadrupole triplet and one skew quadrupole triplet. Angular scattering during stripping was included. The beam line decoupling performance was found to be very stable wrt the magnetic field strength of the solenoid, i.e., the same decoupling gradients can be applied for a wide range of solenoid fields without relevant reduction of the decoupling performance. After the beam is decoupled its rms Twiss parameters α_x, β_x, α_y, β_y do not practically depend on the solenoid field strength that created the coupling. Although the results were illustrated using specific beam parameters, they apply for any other set of beam parameters transported through the proposed kind of beam line. For the time being we can explain the result for a generic case but not the generality of which it has been observed.

ACKNOWLEDGMENTS

This work is supported by the Helmholtz International Center for FAIR and the Bundesministerium für Bildung und Forschung. One of the authors, Chen Xiao, would like to express his sincere thanks to Brahim Mustapha and Peter Ostroumov at ANL and Ina Pschorn at GSI for their fruitful discussions and great help.

APPENDIX A: EIGEN-EMITTANCE FORMULA

Based on linear algebra basics, one has

$$\det(A_1A_2) = \det(A_1)\det(A_2), \tag{A1}$$

$$\det(A_1^T) = \det(A_1), \tag{A2}$$

$$\mathrm{tr}(A_1A_2A_3) = \mathrm{tr}(A_3A_1A_2) = \mathrm{tr}(A_2A_3A_1). \tag{A3}$$

Assuming M is a symplectic transformation, and ε_1 and ε_2 are the eigen-emittances. We use

$$\det(\bar{C}) = \det(MCM^T) = \det(M)\det(C)\det(M^T) \tag{A4}$$

and

$$\det(M) = \det(M^T) = 1 \tag{A5}$$

to obtain

$$\det(C) = (\varepsilon_1\varepsilon_2)^2. \tag{A6}$$

It is straightforward that

$$\begin{aligned}\mathrm{tr}[(\bar{C}J)^2] &= \mathrm{tr}(MCM^TJ \cdot MCM^TJ)\\ &= \mathrm{tr}(MC \cdot M^TJM \cdot CM^TJ)\\ &= \mathrm{tr}(MC \cdot J \cdot CM^TJ)\\ &= \mathrm{tr}(M^TJM \cdot CJC)\\ &= \mathrm{tr}[(JC)^2] = \mathrm{tr}[(CJ)^2]\end{aligned} \tag{A7}$$

and

$$\mathrm{tr}[(CJ)^2] = \mathrm{tr}[(\bar{C}J)^2] = -2(\varepsilon_1^2 + \varepsilon_2^2) \tag{A8}$$

resulting finally in

$$\varepsilon_1 = \tfrac{1}{2}\sqrt{-\mathrm{tr}[(CJ)^2] + \sqrt{\mathrm{tr}^2[(CJ)^2] - 16\det(C)}}, \tag{A9}$$

$$\varepsilon_2 = \tfrac{1}{2}\sqrt{-\mathrm{tr}[(CJ)^2] - \sqrt{\mathrm{tr}^2[(CJ)^2] - 16\det(C)}}. \tag{A10}$$

APPENDIX B: BEAM LINE PARAMETERS

A D_6^+ beam of 11.4 MeV/u is stripped in a foil to a $3D_2^+$ beam. The total relative momentum spread is less than $\pm 5 \times 10^{-4}$. The parameters of the beam line are listed in Table I. Positive gradient means horizontal focusing and a skew refers to a regular quadrupole rotated clockwise by

TABLE I. The lattice of the EMTEX beam line.

Element	Effective length [mm]	Gradient [T/m]
Drift	240.5	
Quad	319	+7.276
Drift	203	
Quad	319	−7.726
Drift	4000	
Quad	354	−0.187
Drift	167.5	
Quad	354	+3.287
Drift	500	
Drift	300	
Half sol	100	+1.00 T
Foil	0	22 μg/cm^2, $\Delta\varphi = 0.226$ mrad
Half sol	100	+1.00 T
Drift	300	
Drift	200	
Quad	319	+10.464
Drift	201	
Quad	319	−9.431
Drift	201	
Quad	319	+8.421
Drift	500	
Skew quad	200	+5.110
Drift	20	
Skew quad	400	−2.229
Drift	20	
Skew quad	200	+8.861
Drift	500	
Quad	200	−7.016
Drift	20	
Quad	400	+7.429
Drift	20	
Quad	200	−7.806
Drift	1289	

TABLE II. The beam parameters at the entrance and exit of the EMTEX beam line. An initial water-bag distribution was assumed for the tracking simulations.

Parameters	Entrance	Exit
α_x/α_y	$-1.21/-2.28$	0.00/0.00
β_x/β_y [mm/mrad]	21.80/15.01	7.18/7.13
$\varepsilon_x/\varepsilon_y$ [mm mrad]	0.509/0.510	0.256/1.144

45° around the beam direction. The decoupling section starts at the exit of the solenoid and ends behind the last skew quadrupole. The beam parameters at the entrance and exit of the beam line are listed in Table II.

[1] R. Brinkmann, Y. Derbenev, and K. Flöttmann, Phys. Rev. ST Accel. Beams **4**, 053501 (2001).

[2] D. Edwards, H. Edwards, N. Holtkamp, S. Nagaitsev, J. Santucci, R. Brinkmann, K. Desler, K. Flöttmann, I. Bohnet, and M. Ferrario, in *Proceedings of the XX International Linac Conference, Monterey, CA, 2000* (SLAC, Menlo Park, CA, 2000), p. 122.

[3] B. E. Carlsten, K. Bishofberger, L. D. Duffy, S. J. Russell, R. D. Ryne, N. A. Yampolsky, and A. J. Dragt, Phys. Rev. ST Accel. Beams **14**, 034002 (2011).

[4] B. E. Carlsten, K. Bishofberger, S. J. Russell, R. D. Ryne, and N. A. Yampolsky, Phys. Rev. ST Accel. Beams **14**, 084403 (2011).

[5] P. Piot, Y.-E. Sun, and K.-J. Kim, Phys. Rev. ST Accel. Beams **9**, 031001 (2006).

[6] P. Piot, Y.-E. Sun, J. G. Power, and M. Rihaoui, Phys. Rev. ST Accel. Beams **14**, 022801 (2011).

[7] Y.-E. Sun, P. Piot, A. Johnson, A. H. Lumpkin, T. J. Maxwell, J. Ruan, and R. Thurman-Keup, Phys. Rev. Lett. **105**, 234801, (2010).

[8] D. Xiang and A. Chao, Phys. Rev. ST Accel. Beams **14**, 114001 (2011).

[9] A. Burov, in *Proceedings of the 52nd ICFA Advanced Beam Dynamics Workshop, Beijing, People's Republic of China*, edited by J. Wang (Institute of High Energy Physics, Beijing, People's Republic of China, 2012).

[10] A. Burov, arXiv:1301.7743.

[11] P. Bertrand, J. P. Biarotte, and D. Uriot, in *Proceedings of the 10th European Particle Accelerator Conference, Edinburgh, Scotland,*, edited by J. Poole and Christine Petit-Jean-Genaz (Institute of Physics, Edinburgh, Scotland, 2006).

[12] A. J. Dragt, Phys. Rev. A **45**, 2572 (1992).

[13] L. Groening, Phys. Rev. ST Accel. Beams **14**, 064201 (2011).

[14] H. Okuno, N. Fukunishi, A. Goto, H. Hasabe, H. Imao, O. Kamigaito, M. Kase, H. Kuboki, Y. Yano, S. Yokouchi, Phys. Rev. ST Accel. Beams **14**, 003503 (2011).

[15] Y. Momozaki, J. Nolen, C. Reed, V. Novick, and J. Specht, JINST **4**, P04005 (2009).

[16] W. Barth, G. Clemente, L. Dahl, P. Gerhard, L. Groening, B. Lommel, M. S. Kaiser, M. Maier, S. Mickat, W. Vinzenz, and H. Vormann, in *Proceeding of the XXIV Linear Accelerator Conference, Victoria, BC, Canada*, edited by M. Comyn (TRIUMF, Victoria, 2008).

[17] A. A. Mullan and W. G. Graham, J. Phys. D **24**, 1533 (1991).

[18] R. Hollinger, P. Beller, K. Volk, M. Weber, and H. Klein, Rev. Sci. Instrum. **71**, 836 (2000).

[19] http://web-docs.gsi.de/weick/atima/.

[20] K.-J. Kim, Phys. Rev. ST Accel. Beams **6**, 104002 (2003).

[21] C. Xiao, L. Groening, and O. Kester, Institute of Applied Physics Internal Report No. IAP-DYNA-190412, 2012.

[22] C. Xiao, L. Groening, and O. Kester, in Proceedings of the 52nd ICFA Advanced Beam Dynamics Workshop, Beijing, People's Republic of China (Ref. [9]).

[23] A. Burov, S. Nagaitsev, A. Shemyakin, and Ya. Derbenev, Phys. Rev. ST Accel. Beams **3**, 094002 (2000).

[24] A. Burov, S. Nagaitsev, and Ya. Derbenev, Phys. Rev. E **66**, 016503 (2002).

[25] P. N. Ostroumov, TRACK version-37, user manual, http://www.phy.anl.gov/atlas/TRACK/.